Highly Wavelength-Selective Enhancement of Responsivity in Ag Nanoparticle-Modified ZnO UV Photodetector

Xiao Wang,[†,‡] Kewei Liu,*,[†] Xing Chen,[†] Binghui Li,[†] Mingming Jiang,[†] Zhenzhong Zhang,[†] Haifeng Zhao,[†] and Dezhen Shen*,[†]

[†]State Key Laboratory of Luminescence and Applications, Changchun Institute of Optics, Fine Mechanics and Physics, Chinese Academy of Sciences, Changchun 130033, People's Republic of China

[‡]Graduate University of the Chinese Academy of Sciences, Beijing 100049, People's Republic of China

Ⓢ Supporting Information

ABSTRACT: We proposed and demonstrated Ag nanoparticles (NPs)-decorated ZnO photodetectors for UV light sensing. After decoration of their surface with random Ag NPs, the dark current density of ZnO UV photodetectors decreases obviously. Moreover, the device exhibits an obvious increase in peak responsivity at around 380 nm, which can be attributed to the narrow-band quadrupole plasmon resonance of Ag NPs in the UV range. Meanwhile, the responsivity at the other wavelengths decreases a lot. As a result, the response peak becomes more significant, and the response of the devices presents an excellent wavelength selectivity after covering with Ag NPs. The detailed mechanism for this phenomenon was explained. We believe that our findings would open a way to harness the high-order plasmon modes in the field of UV optoelectronic devices.

KEYWORDS: surface plasmon resonance, semiconductor, quadrupole, wide band gap, solar-blind
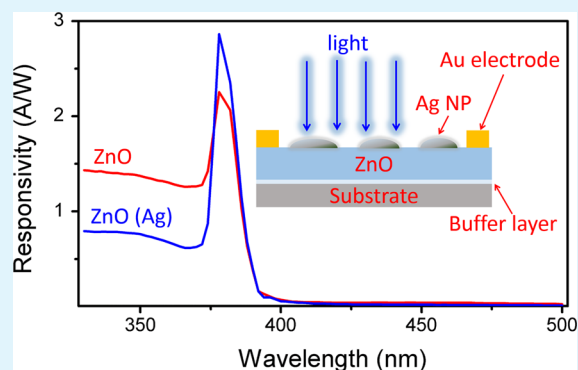
1. INTRODUCTION

The UV-detection technique has a wide application in both military and civilian fields, such as plume sensing, space exploration, environmental monitoring, flame detection, etc.[1,2] The core of the UV-detection technique is the high-performance UV detector. In recent years, wide-bandgap semiconductor UV photodetectors have received more and more attention due to their intrinsic visible blindness, high radiation hardness, lack of need for any filters or refrigeration, and so on.[3−5] Thus, they are expected to replace the traditional vacuum photomultiplier tubes and Si photomultipliers, becoming a new generation of UV photodetectors.[6−10] Among the wide-bandgap semiconductors, ZnO-based materials have relatively lower defect density, higher saturated carrier drift rate, and stronger radiation hardness.[11−13] Moreover, by alloying ZnO with MgO to form ternary ZnMgO, the band gap can be tuned from 3.37 to 7.8 eV at room temperature.[14−16] Therefore, ZnO-based semiconductors are regarded as one of the most ideal materials to prepare the solar-blind and visible-blind UV photodetectors.[17−22] However, owing to the immaturity of p-type doping and other related technology, the performance of ZnO-based UV photodetectors is still lower than expected. For the fabrication of high-performance ZnO-based UV photodetectors, a common and effective method is improving the materials quality and optimizing the device technology, but this is usually a long-term process. Alternatively, combining with other effects or methods to improve

the performance of existing devices should be a more-efficient and feasible option. Plasma-enhanced semiconductor photodetector is one of the most typical representatives,[23−25] and surface plasmon resonance (SPR) from the metallic nanostructures can effectively improve the performance of photodetectors.[26−34] According to the previous reports, the key factor for SPR enhancement is the energy match between SPR and detection wavelength.[24,25] The dipole resonance, as the most easily realized mode among the SPR modes, is usually demonstrated in the visible and near-infrared spectral regions for most metals,[25,35] and thus, the previous performance enhancements were primarily observed in these wavelength ranges.[28,29] Therefore, for the realization of the plasmon-enhanced UV photodetectors, the first thing is to solve the energy mismatching problem, namely extending the plasmon resonance frequency into UV region. Reducing the size of metallic nanostructures could realize a blue-shift of dipole resonance frequency,[36,37] but it is limited by the nano-fabrication techniques, and the smaller-size nanostructures usually have larger ratio of absorption to scattering, which is not conducive to improving the performance of the photodetectors.[37] Compared to the traditional dipole plasmon resonance, high-order plasmon modes are often excited in the

shorter-wavelength regime, which is expected to be used to improve the UV-detection performance. However, multipoles are usually difficult to be realized, and the related research is very little. Recently, our group found that a narrow-band hybridized quadrupole resonance can be demonstrated in the UV range in random Ag nanoclusters.[38−40] More interestingly, this quadrupole resonance could strongly couple with the near-band-edge (NBE) excitons of ZnMgO, resulting in a giant UV-emission enhancement.[39,40] Nevertheless, no information can be found about the effect of high-order plasmon resonances on the UV-detection performance until now.

In this paper, we report a performance enhancement of ZnO UV photodetectors by the random Ag nanoparticles (NPs). After decoration of their surface with Ag NPs, the dark current density of ZnO UV photodetectors decreases obviously. More interestingly, the response spectrum shows an obvious change: the peak responsivity at around 380 nm increases, while the responsivity at the other wavelength regions decreases. The highly wavelength-selective UV response enhancement for ZnO photodetectors can be attributed to the narrow-band quadrupole resonance in Ag NPs. To the best of our knowledge, this device is the first plasmon-enhanced photodetector, determined based on high-order plasmon resonance.

2. EXPERIMENTAL SECTION

ZnO films were deposited on c-face sapphire substrate by plasma-assisted molecular beam epitaxy (P-MBE). Prior to growth, the substrates were treated by N_2 at 950 °C for 60 min to remove possible absorbed contaminants. 6N-purity zinc held in thermal Knudsen cells and 5N-purity O_2 activated in a radio frequency (RF) plasma source were employed as precursors. A thin ZnO buffer layer was deposited at 550 °C. Subsequently, the substrate temperature was increased to 850 °C to stabilize the buffer layer. Then, high-quality ZnO films were grown with the substrate temperature of 750 °C and the pressure in the chamber of 10^{-5} Pa. The Zn source temperature was fixed at 500 °C and the RF source power was kept at 250 W. After that, Ag (99.99%) was deposited on the surface of ZnO film by a radio frequency magnetron sputtering technique at room temperature, which was subsequently annealed in N_2 atmosphere at 450 °C for 20 min to form Ag NPs. The N_2 flow rate was fixed at 200 mL/min. The surface morphology of the samples was measured by scanning electron microscope (SEM) (HITACHI S-4800). The structural properties were investigated by D/max-RA X-ray diffraction (XRD) (Rigaku) with Cu $K\alpha$ as the radiation source (λ = 0.154 nm). The extinction, transmission, and absorption spectra were recorded by a UV-3101PC scanning spectrophotometer. Photoluminescence (PL) spectra of the samples were measured at room temperature using an integrating sphere excited by a continuous-wave He−Cd laser (325 nm).

Au (∼30 nm thick) electrodes were deposited to realize Ag plasmon-enhanced ZnO metal−semiconductor-metal (MSM) UV photodetectors by a sputtering method at room temperature. The schematic device structure is shown in Figure 1a. A pair of electrodes with the distance of 2 mm were realized by photolithography and lift-off technique. A device with the same structure based on 450 °C annealed bare ZnO film was used as control sample. The current density−voltage (J−V) properties and spectral responses of the fabricated devices were measured using a semiconductor parameter analyzer (Keithley 2200) and 200 W UV-enhanced Xe lamp with a monochromator, respectively.

3. RESULTS AND DISCUSSION

Figure 1b shows the XRD pattern of the ZnO films with and without Ag NPs. The peak observed at 41.66° for the Cu $K\alpha1$ line corresponds to (0006) Al_2O_3 peak from the substrate. Besides the substrate diffraction peak, the peak located at 34.44° for the Cu $K\alpha1$ line can be assigned to the (0002)
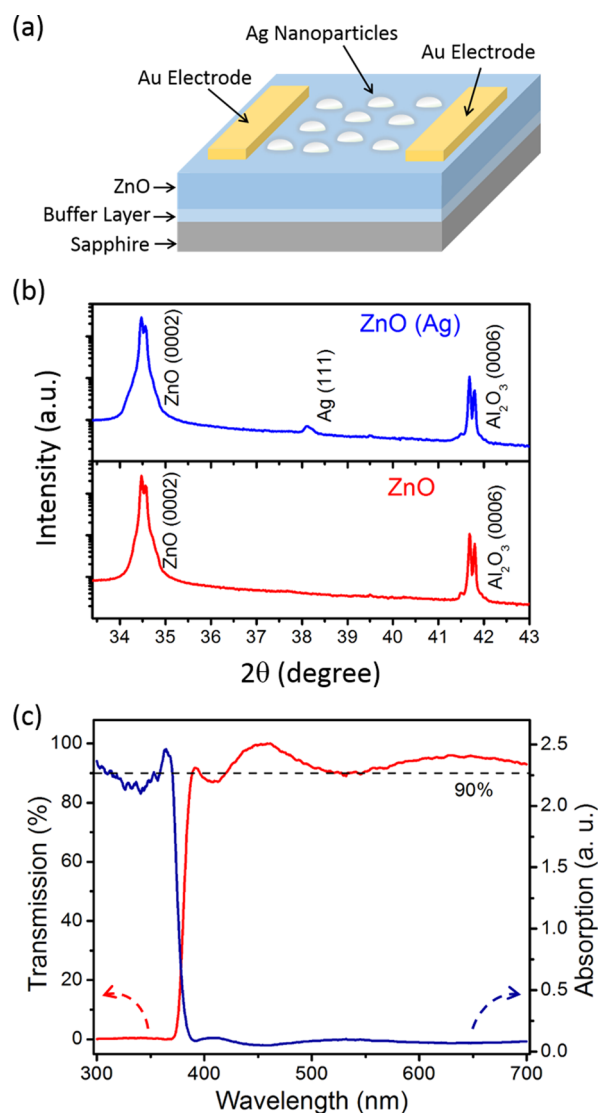

Figure 1. (a) Schematic structure of the ZnO-based UV photo-detector. (b) XRD patterns of ZnO films with and without Ag NPs. (c) Transmission and absorption spectra of the ZnO film.

orientation of wurtzite ZnO. The narrow peak indicates very good crystalline quality of ZnO. After covering with Ag NPs, a new weak peak appeared at 38.1°, which can be attributed to (111) diffraction plane of face-centered cubic structured Ag.[41] Figure 1c shows the transmission and absorption spectra of the ZnO film on sapphire substrate. It is clear that the sample has more than 90% average transmission in the visible region and has a very sharp absorption edge at ∼370 nm. A pronounced exciton peak can be clearly observed near the absorption edge, suggesting a high crystalline quality of ZnO.[42,43]

Figures 2a,b shows the SEM images of the surface morphology of ZnO film with and without Ag NPs, respectively. It is obvious that ZnO films have rough surface with nanonetwork structures. Moreover, Ag NPs show obvious sphere-like shape with the diameter of 150−350 nm and the average interspace of 500−800 nm. Figure 3 presents the experimental extinction spectra of ZnO films with and without Ag NPs. It can be found that an obvious increase of ZnO exciton absorption peak in the UV range and the emergence of a broad visible extinction band are realized by covering with Ag NPs. To understand this phenomenon, the finite difference
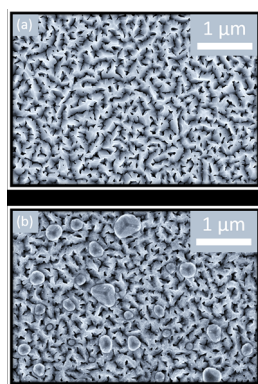
Figure 2. SEM images of the surface morphology of (a) bare ZnO film and (b) Ag-modified ZnO film.
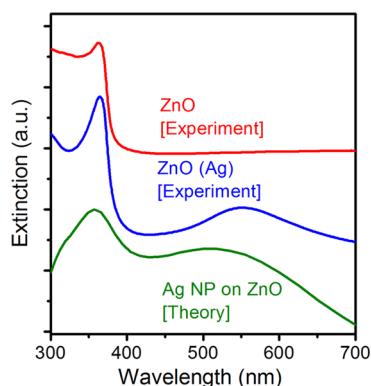
Figure 3. Experimental extinction spectra of bare ZnO film and Ag-decorated ZnO film and simulated extinction spectra of the isolated Ag nanosphere with the diameter of 200 nm on the surface of ZnO film.

time-domain (FDTD) simulations were carried out. The simulated extinction spectrum of the isolated Ag nanosphere with the diameter of 200 nm on ZnO film is also shown in Figure 3. A relatively narrow quadrupole plasmon resonance peak and a broad dipole plasmon resonance band can be clearly observed at UV and visible regions, respectively. Moreover, with increasing the diameter of Ag NPs from 150 to 300 nm, a strong blue shift of the dipolar resonance and a weak blue shift of the quadrupole resonance can be observed (see Figure S1). The experiment shows a comparatively good agreement with the simulated spectrum, and a slight peak shift may be induced by the roughness of the ZnO top surface and the random nature of Ag NPs. Additionally, Ag NPs on sapphire with the similar morphology to that on ZnO film also present both quadrupole and dipole resonances, as shown in Figure S2. Therefore, an obvious increase of ZnO exciton absorption peak in the UV range and the emergence of a broad visible extinction band for Ag-decorated ZnO film can be attributed to the quadrupole and dipole resonances of Ag NPs, respectively.

To further investigate the optical properties of the samples, PL measurements were carried out on ZnO and ZnO (Ag) films at room temperature as shown in Figure 4. The inset is the schematic arrangement of the PL measurement configuration. The strong narrow PL peak at around 382 nm corresponds to the NBE emission of the ZnO film, and a small emission shoulder at its shorter wavelength side may come from the nanonetwork structured surface of ZnO due to the quantum confinement effect. In addition, nearly no visible emission can be observed. Interestingly, ZnO (Ag) shows an
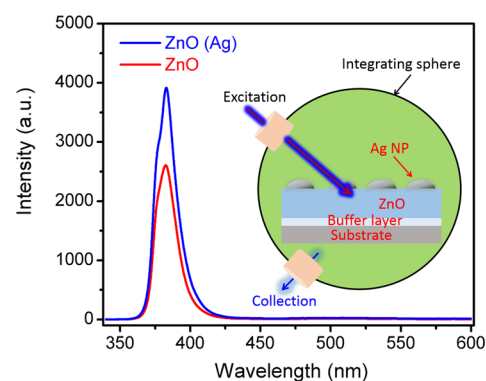
Figure 4. Room-temperature PL spectra of the ZnO film with and without Ag NPs. The inset is the excitation and collection configuration.

obvious intensity enhancement for UV emission, which is in good agreement with our previous reports.[39,40] A strong coupling between ZnO NBE UV emission and Ag quadrupole resonance should be responsible for this enhancement due to their excellent energy match (see Figure 5). Notably, in this
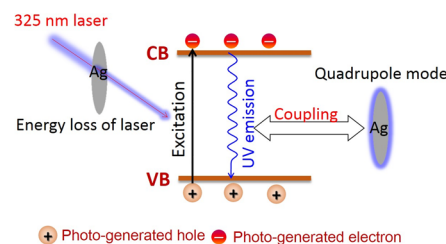

Figure 5. Schematic diagram for carrier generation and recombination of ZnO films with Ag NPs. The transition from the conduction band (CB) to the valence band (VB) for the UV emission is illustrated. The energy loss of laser-induced by shading effect of Ag NPs and the coupling between UV-light emission from ZnO and Ag quadrupole plasmon resonance are shown.

case, the sample was excited from the metal side (see the inset of Figure 4); thus, the energy loss of incident light should be significant due to the shading effect of Ag. As a result, after covering with Ag NPs, the number of photons absorbed by ZnO should be significantly decreased, resulting in a decrease in the number of photogenerated carriers. Thus, the shading effect of Ag NPs would decrease the UV emission intensity of ZnO. In theory, the UV emission of ZnO (Ag) should get stronger without shading effect.

Based on the above-mentioned ZnO films with and without Ag NPs, a serious MSM UV photodetectors have been demonstrated. To explore the effect of Ag NPs on the performance of ZnO photodetectors, the measurements of $J-V$ curves and response spectra have been carried out on the devices based on ZnO films with and without Ag NPs. Figure. 6a shows the $J-V$ characteristics of the devices, both in the dark and under UV-light irradiation (380 nm). The linearity of the $J-V$ curves in the dark indicates that the contact between the ZnO film and Au electrode is an ohmic contact. Additionally, it can be found that the dark current density decreases from 60 to 38 mA/cm² at 5 V after covering with Ag NPs. This phenomenon can be attributed to the localized Schottky junction between ZnO and Ag.[44] As is well-known, the work function of Ag is 4.26 eV, and the electron affinity of ZnO is 4.2
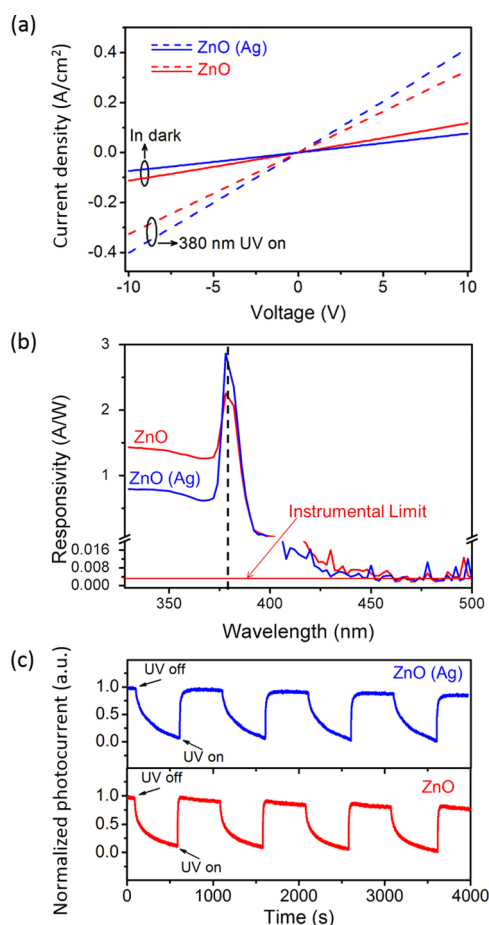
Figure 6. (a) J−V characteristics in dark condition and (b) response spectra of the ZnO UV photodetectors with and without Ag NPs under 15 V bias. (c) Time-dependent photocurrent with periodic switching of UV illumination (380 nm) measured at 30 V bias.

eV.[45] When Ag metal contacts with ZnO, a localized Schottky junction can be formed at the interface, depleting the carriers near the surface of ZnO. The formation of this depletion region should be the main reason for the decrease in the dark current. Interestingly, when exposed to 380 nm UV irradiation, both devices show apparent photoresponse. However, the current increase of the ZnO film coated with Ag NPs is larger than that of bare ZnO film.

The spectral response of the device was measured using a 200 W Xe lamp, monochromator, chopper, and lock-in amplifier. Figure 6b shows the response spectra of the ZnO UV photodetectors with and without Ag NPs under 15 V bias. The −3 dB cutoff edge is around 385 nm for both devices, which is in good accordance with the result of UV−visible

transmission and absorption spectra of ZnO in Figure 1c. Notably, the sharp peak appear at a wavelength of ∼380 nm, indicating that the excitons generated in the ZnO film contribute to the photocurrent through the dissociation of the excitons. The dissociation of excitons should be induced by the strong electric field between two electrodes. More interestingly, after covering with Ag NPs, the intensity of the response peak increases obviously from 2.16 to 2.86 A/W, while the responsivity at the other wavelengths decreases a lot. As a result, the response peak becomes more significant with a spectral width of $\Delta\lambda$ = 10 nm (full width at half-maximum, fwhm) after covering by Ag NPs, and the response of the devices present excellent wavelength selectivity. These phenomena can be explained as follow. Considering a large energy match between the excitonic absorption peak of ZnO and the quadrupole plasmon resonance peak of Ag NPs, it can be concluded that the increase of the peak photoresponsivity for the Ag-decorated device should be attributed to the strong incident light scattering. As for the wavelength range shorter than 370 nm, the shading effect of Ag NPs results in a decrease in the light absorption of ZnO, thus reducing the responsivity. Additionally, the responsivity of two devices decreased sharply with an increase in the wavelength from 380 to 390 nm and reached the instrumental limit (∼0.002 A/W) at a wavelength of 460 nm. The UV−visible rejection, defined as the ratio between the peak responsivity and responsivity at 500 nm, is as large as 10^3. It is worth mentioning that the fabrication and the performance of the device with and without Ag present excellent reproducibility (see Table S1).

Response speed and repeatability are important factors when determining the alerting ability of a photodetector. We investigated time-dependent photocurrent with the 380 nm light switched on and off for the ZnO UV photodetectors with and without Ag NPs under 30 V bias, as shown in Figure 6c. The on−off switching properties of the device is shown under light illumination with a 380 nm wavelength; with both on and off time set at 500 s, it can be seen that both devices exhibit good on−off switching performance with high stability and reproducibility. The response time (raise time) was defined as the time to reach 90% of the maximum photocurrent after switching on the light, and the recovery time (decay time) was extracted from the time to reach 10% of the photocurrent after switching off the light. The raise time and decay time of the ZnO UV photodetector were estimated to be ∼15 and ∼330 s, respectively. After covering with Ag NPs, no obvious change in response speed can be observed. The performance parameters of the ZnO UV photodetectors of present and previous works are summarized in Table 1. The response speed of our devices is slower than that of previous reported devices,[46,47] which should be associated with the slow O_2 adsorption and

Table 1. Summary of Key Parameters of ZnO-Based UV Photodetectors Reported in the Past 3 Years

device	dark current (density)	peak responsivity	fwhm of response peak (nm)	raise time/decay time (s)	ref
ZnO−Si heterojunction	4 μA @−10 V	0.38 A/W @360 nm	−	11/14	46
ZnO NW	∼250 μA @5 V	∼6 A/W	−	9.5/38	47
ZnO film	2.75 μA @15 V	67.8 mA/W	−	−	49
ZnO NP networks	<5 nA @5 V	∼13 A/W @370 nm	∼70	∼250/∼150	50
Au−ZnO NRs heterojunction	∼50 nA @−3 V	5.65 mA/W @365 nm	∼160	−	51
CuSCN−ZnO NRs heterojunction	∼5 nA @−3 V	22.5 mA/W @365 nm	∼50	−	51
ZnO film	60 mA/cm^2 @5 V	2.16 A/W @380 nm	−	∼15/∼330	this work
ZnO film with Ag NPs	38 mA/cm^2 @5 V	2.86 A/W @380 nm	∼10	∼15/∼330	this work

desorption processes on the nanonetwork structured surface of ZnO film.[44,48] Additionally, the fwhm of the response peak for Ag NPs-decorated device is only around 10 nm, which is much narrower than that of other ZnO photodetectors.[50,51]

4. CONCLUSIONS

In this paper, Ag-NPs-coated ZnO photodetectors have been demonstrated by MBE with excellent wavelength selectivity. After covering with Ag NPs, the dark current density of ZnO UV detector decreases from 60 to 38 mA/cm^2, which can be attributed to the localized Schottky junction between ZnO film and Ag NPs. More interestingly, the intensity of the response peak at around 380 nm increases obviously, while the responsivity at the other wavelengths decreases a lot. The extinction and PL spectra indicated that the strong incident light scattering due to the quadrupole plasmon resonance of Ag NPs should be responsible for the peak responsivity enhancement. As for the suppression of the response at the other wavelengths, it should be associated with the shading effect and the surface defect passivation of Ag NPs. Consequently, for the first time, the UV responsivity was selectively improved by high-order plasmon mode in this work, and the fwhm of response peak for Ag NPs-decorated device is as narrow as around 10 nm. In addition, the raise time and decay time of the ZnO UV photodetector were estimated to be ∼15 and ∼330 s, respectively. Our results could provide a promising way to develop high-performance UV photodetectors with high spectral selectivity.

ASSOCIATED CONTENT

ⓢ Supporting Information

The Supporting Information is available free of charge on the ACS Publications website at DOI: 10.1021/acsami.6b14430.

> Figures showing simulated extinction spectra of the isolated Ag nanosphere with different diameter on the surface of ZnO film and an SEM image and extinction spectrum of Ag NPs grown on sapphire substrate with the sputtering time of 7 min. A table showing responsivity at 340 and 380 nm of ZnO ultraviolet photodetectors with and without Ag nanoparticles under a 15 V bias. (PDF)

AUTHOR INFORMATION

Corresponding Authors
*E-mail: liukw@ciomp.ac.cn.
*E-mail: shendz@ciomp.ac.cn.
ORCID ⓘ
Xiao Wang: 0000-0002-5377-0813

Author Contributions
The manuscript was written through contributions of all authors. All authors have given approval to the final version of the manuscript.

Notes
The authors declare no competing financial interest.

ACKNOWLEDGMENTS

REFERENCES

(1) Razeghi, M.; Rogalski, A. Semiconductor Ultraviolet Detectors. *J. Appl. Phys.* **1996**, *79*, 7433−7473.

(2) Chen, H. Y.; Liu, H.; Zhang, Z. M.; Hu, K.; Fang, X. S. Nanostructured Photodetectors: from Ultraviolet to Terahertz. *Adv. Mater.* **2016**, *28*, 403−433.

(3) Morkoc, H.; Strite, S.; Gao, G. B.; Lin, M. E.; Sverdlov, B.; Burns, M. Large-Band-Gap SiC, III-V Nitride, and II-VI ZnSe-Based Semiconductor-Device Technologies. *J. Appl. Phys.* **1994**, *76*, 1363−1398.

(4) Monroy, E.; Omnès, F.; Calle, F. Wide-Bandgap Semiconductor Ultraviolet Photodetectors. *Semicond. Sci. Technol.* **2003**, *18*, R33−R51.

(5) Zhai, T. Y.; Li, L.; Ma, Y.; Liao, M. Y.; Wang, X.; Fang, X. S.; Yao, J. N.; Bando, Y.; Golberg, D. One-Dimensional Inorganic Nanostructures: Synthesis, Field-Emission and Photodetection. *Chem. Soc. Rev.* **2011**, *40*, 2986−3004.

(6) Parish, G.; Keller, S.; Kozodoy, P.; Ibbetson, J. P.; Marchand, H.; Fini, P. T.; Fleischer, S. B.; DenBaars, S. P.; Mishra, U. K.; Tarsa, E. J. High-Performance (Al,Ga)N-Based Solar-Blind Ultraviolet p-i-n Detectors on Laterally Epitaxially Overgrown GaN. *Appl. Phys. Lett.* **1999**, *75*, 247−249.

(7) Monroy, E.; Palacios, T.; Hainaut, O.; Omnès, F.; Calle, F.; Hochedez, J. F. Assessment of GaN Metal-Semiconductor-Metal Photodiodes for High-Energy Ultraviolet Photodetection. *Appl. Phys. Lett.* **2002**, *80*, 3198−3200.

(8) Liao, M. Y.; Koide, Y. High-Performance Metal-Semiconductor-Metal Deep-Ultraviolet Photodetectors Based on Homoepitaxial Diamond Thin Film. *Appl. Phys. Lett.* **2006**, *89*, 113509.

(9) Chen, X. P.; Zhu, H. L.; Cai, J. F.; Wu, Z. Y. High-Performance 4H-SiC-Based Ultraviolet p-i-n Photodetector. *J. Appl. Phys.* **2007**, *102*, 024505.

(10) Bie, Y. Q.; Liao, Z. M.; Zhang, H. Z.; Li, G. R.; Ye, Y.; Zhou, Y. B.; Xu, J.; Qin, Z. X.; Dai, L.; Yu, D. P. Self-Powered, Ultrafast, Visible-Blind UV Detection and Optical Logical Operation Based on ZnO/GaN Nanoscale p-n Junctions. *Adv. Mater.* **2011**, *23*, 649−653.

(11) Ozgür, U.; Alivov, Y. I.; Liu, C.; Teke, A.; Reshchikov, M. A.; Dogan, S.; Avrutin, V.; Cho, S. J.; Morkoç, H. A Comprehensive Review of ZnO Materials and Devices. *J. Appl. Phys.* **2005**, *98*, 041301.

(12) Hou, Y. N.; Mei, Z. X.; Du, X. L. Semiconductor Ultraviolet Photodetectors Based on ZnO and Mg$_x$Zn$_{1-X}$O. *J. Phys. D: Appl. Phys.* **2014**, *47*, 283001.

(13) Liu, K. W.; Sakurai, M.; Aono, M. ZnO-Based Ultraviolet Photodetectors. *Sensors* **2010**, *10*, 8604−8634.

(14) Koike, K.; Hama, K.; Nakashima, I.; Takada, G.; Ogata, K.; Sasa, S.; Inoue, M.; Yano, M. Molecular Beam Epitaxial Growth of Wide Bandgap ZnMgO Alloy Films on (111)-Oriented Si Substrate Toward UV-detector Applications. *J. Cryst. Growth* **2005**, *278*, 288−292.

(15) Boutwell, R. C.; Wei, M.; Schoenfeld, W. V. The Effect of Substrate Temperature and Source Flux on Cubic ZnMgO UV Sensors Grown by Plasma-Enhanced Molecular Beam Epitaxy. *Appl. Surf. Sci.* **2013**, *284*, 254−257.

(16) Boutwell, R. C.; Wei, M.; Schoenfeld, W. V. The Effect of Oxygen Flow Rate and Radio Frequency Plasma Power on Cubic ZnMgO Ultraviolet Sensors Grown by Plasma-Enhanced Molecular Beam Epitaxy. *Appl. Phys. Lett.* **2013**, *103*, 031114.

(17) Wang, L. K.; Ju, Z. G.; Zhang, J. Y.; Zheng, J.; Shen, D. Z.; Yao, B.; Zhao, D. X.; Zhang, Z. Z.; Li, B. H.; Shan, C. X. Single-Crystalline Cubic MgZnO Films and Their Application in Deep-Ultraviolet Optoelectronic Devices. *Appl. Phys. Lett.* **2009**, *95*, 131113.

(18) Fan, M. M.; Liu, K. W.; Chen, X.; Wang, X.; Zhang, Z. Z.; Li, B. H.; Shen, D. Z. Mechanism of Excellent Photoelectric Characteristics in Mixed-Phase ZnMgO Ultraviolet Photodetectors with Single Cutoff Wavelength. *ACS Appl. Mater. Interfaces* **2015**, *7*, 20600−20606.

(19) Boruah, B. D.; Mukherjee, A.; Misra, A. Sandwiched Assembly of ZnO Nanowires between Graphene Layers for a Self-Powered and Fast Responsive Ultraviolet Photodetector. *Nanotechnology* **2016**, *27*, 095205.

(20) Kim, D. Y.; Ryu, J.; Manders, J.; Lee, J.; So, F. Air-Stable, Solution-Processed Oxide p-n Heterojunction Ultraviolet Photodetector. *ACS Appl. Mater. Interfaces* **2014**, *6*, 1370−1374.

(21) Su, L. X.; Zhu, Y.; Yong, D. Y.; Chen, M. M.; Ji, X.; Su, Y. Q.; Gui, X. C.; Pan, B. C.; Xiang, R.; Tang, Z. K. Wide Range Bandgap Modulation Based on ZnO-Based Alloys and Fabrication of Solar Blind UV Detectors with High Rejection Ratio. *ACS Appl. Mater. Interfaces* **2014**, *6*, 14152−14158.

(22) Zhang, H.; Hu, Y. F.; Wang, Z. P.; Fang, Z. Y.; Peng, L. M. Performance Boosting of Flexible ZnO UV Sensors with Rational Designed Absorbing Antireflection Layer and Humectant Encapsulation. *ACS Appl. Mater. Interfaces* **2016**, *8*, 381−389.

(23) Zia, R.; Schuller, J. A.; Chandran, A.; Brongersma, M. L. Plasmonics: the Next Chip-Scale Technology. *Mater. Today* **2006**, *9*, 20−27.

(24) Barnes, W. L.; Dereux, A.; Ebbesen, T. W. Surface Plasmon Subwavelength Optics. *Nature* **2003**, *424*, 824−830.

(25) Ozbay, E. Plasmonics: Merging Photonics and Electronics at Nanoscale Dimensions. *Science* **2006**, *311*, 189−193.

(26) Chalabi, H.; Schoen, D.; Brongersma, M. L. Hot-Electron Photodetection with a Plasmonic Nanostripe Antenna. *Nano Lett.* **2014**, *14*, 1374−1380.

(27) Payne, E. K.; Shuford, K. L.; Park, S.; Schatz, G. C.; Mirkin, C. A. Multipole Plasmon Resonances in Gold Nanorods. *J. Phys. Chem. B* **2006**, *110*, 2150−2154.

(28) Wu, W.; Bonakdar, A.; Mohseni, H. Plasmonic Enhanced Quantum Well Infrared Photodetector with High Detectivity. *Appl. Phys. Lett.* **2010**, *96*, 161107−1−161107−3.

(29) Chang, C. C.; Sharma, Y. D.; Kim, Y. S.; Bur, J. A.; Shenoi, R. V.; Krishna, S.; Huang, D. H.; Lin, S. Y. A Surface Plasmon Enhanced Infrared Photodetector Based on InAs Quantum Dots. *Nano Lett.* **2010**, *10*, 1704−1709.

(30) Sheu, J. K.; Lee, M. L.; Lin, Y. C. Surface Plasmon-Enhanced GaN Metal-Insulator-Semiconductor Ultraviolet Detectors with Ag Nanoislands Embedded in a Silicon Dioxide Gate Layer. *IEEE J. Sel. Top. Quantum Electron.* **2014**, *20*, 3801005.

(31) Hu, K.; Chen, H. Y.; Jiang, M. M.; Teng, F.; Zheng, L. X.; Fang, X. S. Broadband Photoresponse Enhancement of a High-Performance t-Se Microtube Photodetector by Plasmonic Metallic Nanoparticles. *Adv. Funct. Mater.* **2016**, *26*, 6641−6648.

(32) Lu, J. F.; Xu, C. X.; Dai, J.; Li, J. T.; Wang, Y. Y.; Lin, Y.; Li, P. L. Improved UV Photoresponse of ZnO Nanorod Arrays by Resonant Coupling with Surface Plasmons of Al Nanoparticles. *Nanoscale* **2015**, *7*, 3396−3403.

(33) Ahmadivand, A.; Sinha, R.; Vabbina, P. K.; Karabiyik, M.; Kaya, S.; Pala, N. Hot Electron Generation by Aluminum Oligomers in Plasmonic Ultraviolet Photodetectors. *Opt. Express* **2016**, *24*, 13665−13678.

(34) Gogurla, N.; Sinha, A. K.; Santra, S.; Manna, S.; Ray, S. K. Multifunctional Au-ZnO Plasmonic Nanostructures for Enhanced UV Photodetector and Room Temperature NO Sensing Devices. *Sci. Rep.* **2014**, *4*, 6483−1−6483−9.

(35) Pelton, M.; Aizpurua, J.; Bryant, G. Metal-Nanoparticle Plasmonics. *Laser Photonics Rev.* **2008**, *2*, 136−159.

(36) Langhammer, C.; Kasemo, B.; Zorić, I. Absorption and Scattering of Light by Pt, Pd, Ag, and Au Nanodisks: Absolute Cross Sections and Branching Ratios. *J. Chem. Phys.* **2007**, *126*, 194702.

(37) Scholl, J. A.; Koh, A. L.; Dionne, J. A. Quantum Plasmon Resonances of Individual Metallic Nanoparticles. *Nature* **2012**, *483*, 421−428.

(38) Jiang, M. M.; Chen, H. Y.; Li, B. H.; Liu, K. W.; Shan, C. X.; Shen, D. Z. Hybrid Quadrupolar Resonances Stimulated at Short Wavelengths Using Coupled Plasmonic Silver Nanoparticle Aggregation. *J. Mater. Chem. C* **2014**, *2*, 56−63.

(39) Chen, H. Y.; Liu, K. W.; Jiang, M. M.; Zhang, Z. Z.; Liu, L.; Li, B. H.; Xie, X. H.; Wang, F.; Zhao, D. X.; Shan, C. X.; Shen, D. Z. Tunable Hybridized Quadrupole Plasmons and Their Coupling with Excitons in ZnMgO/Ag System. *J. Phys. Chem. C* **2014**, *118*, 679−684.

(40) Chen, H. Y.; Liu, K. W.; Jiang, M. M.; Zhang, Z. Z.; Xie, X. H.; Wang, D. K.; Liu, L.; Li, B. H.; Zhao, D. X.; Shan, C. X.; Shen, D. Z. Tunable Enhancement of Exciton Emission from MgZnO by Hybridized Quadrupole Plasmons in Ag Nanoparticle Aggregation. *Appl. Phys. Lett.* **2014**, *104*, 091119.

(41) Li, Y.; Zhang, P.; Ouyang, Z.; Zhang, M.; Lin, Z.; Li, J.; Su, Z.; Wei, G. Nanoscale Graphene Doped with Highly Dispersed Silver Nanoparticles: Quick Synthesis, Facile Fabrication of 3D Membrane-Modified Electrode, and Super Performance for Electrochemical Sensing. *Adv. Funct. Mater.* **2016**, *26*, 2122−2134.

(42) Janotti, A.; Van de Walle, C. G. Fundamentals of Zinc Oxide as a Semiconductor. *Rep. Prog. Phys.* **2009**, *72*, 126501.

(43) Chen, Y. F.; Bagnall, D. M.; Koh, H. J.; Park, K. T.; Hiraga, K.; Zhu, Z. Q.; Yao, T. Plasma Assisted Molecular Beam Epitaxy of ZnO on c-plane Sapphire: Growth and Characterization. *J. Appl. Phys.* **1998**, *84*, 3912−3918.

(44) Liu, K. W.; Sakurai, M.; Liao, M. Y.; Aono, M. Giant Improvement of the Performance of ZnO Nanowire Photodetectors by Au Nanoparticles. *J. Phys. Chem. C* **2010**, *114*, 19835−19839.

(45) Brillson, L. J.; Lu, Y. C. ZnO Schottky Barriers and Ohmic Contacts. *J. Appl. Phys.* **2011**, *109*, 121301.

(46) Al-Hardan, N. H.; Jalar, A.; Hamid, M. A. A.; Keng, L. K.; Ahmed, N. M.; Shamsudin, R. A Wide-Band UV Photodiode Based on n-ZnO/p-Si Heterojunctions. *Sens. Actuators, A* **2014**, *207*, 61−66.

(47) Boruah, B. D.; Mukherjee, A.; Sridhar, S.; Misra, A. Highly Dense ZnO Nanowires Grown on Graphene Foam for Ultraviolet Photodetection. *ACS Appl. Mater. Interfaces* **2015**, *7*, 10606−10611.

(48) Zhang, D. H. Adsorption and Photodesorption of Oxygen on the Surface and Crystallite Interfaces of Sputtered ZnO Films. *Mater. Chem. Phys.* **1996**, *45*, 248−252.

(49) Tian, C. G.; Jiang, D. Y.; Zhao, Y. J.; Liu, Q. F.; Hou, J. H.; Zhao, J. X.; Liang, Q. C.; Gao, S.; Qin, J. M. Effects of Continuous Annealing on the Performance of ZnO Based Metal-Semiconductor-Metal Ultraviolet Photodetectors. *Mater. Sci. Eng., B* **2014**, *184*, 67−71.

(50) Nasiri, N.; Bo, R. H.; Wang, F.; Fu, L.; Tricoli, A. Ultraporous Electron-Depleted ZnO Nanoparticle Networks for Highly Sensitive Portable Visible-Blind UV Photodetectors. *Adv. Mater.* **2015**, *27*, 4336−4343.

(51) Zhang, Y. Z.; Xu, J. P.; Shi, S. B.; Gao, Y. Y.; Wang, C.; Zhang, X. S.; Yin, S. G.; Li, L. Development of Solution-Processed ZnO Nanorod Arrays Based Photodetectors and the Improvement of UV Photoresponse via AZO Seed Layers. *ACS Appl. Mater. Interfaces* **2016**, *8*, 22647−22657.